RSC Advances

ROYAL SOCIETY OF CHEMISTRY

www.rsc.org/advances

RSC Advances

PAPER

Chitosan/organic rectorite nanocomposites rapid synthesized by microwave irradiation: effects of chitosan molecular weight

Siqi Huang,[a] Zhiming Yu,[a] Chusheng Qi,[a] and Yang Zhang*[a]

Chitosans with high and low molecular weight (CSH and CSL) were intercalated into organic rectorite (OREC) to prepare chitosan/organic rectorite nanocomposites (CSHOR and CSLOR) via microwave irradiation method for 75 min, which was found to be much more efficient than the conventional 48-h heating method. The structure and intercalation mechanism of the nanocomposites were investigated by XRD, FT-IR, and zeta potential analysis, and the effects of chitosan (CS) molecular weight on the morphology, crystallization behavior, thermal stability, and antibacterial properties of the nanocomposites were explored. The results indicated that: 1) CSH and CSL were inserted successfully into the silicate layers to form the intercalated nanocomposites, and interlayer spacing could be increased to 5.14 nm and 6.40 nm, respectively. 2) CS and OREC were joined together through hydrogen bonding and electrostatic interaction. 3) Compared to CSH and CSL, the thermal stability and antibacterial properties of both CSHOR and CSLOR were significantly improved. 4) With decreasing CS molecular weight the interlayer distance of OREC increased, which resulted in morphological and crystallization changes of the nanocomposites and enhanced antibacterial activity without impacting thermal stability.

Received 00th January 2015,
Accepted 00th January 2015

DOI: 10.1039/x0xx00000x

www.rsc.org/

Introduction

Biopolymer-clay nanocomposites, which combine the physical and chemical properties of both inorganic and organic materials, have recently garnered much attention from researchers and developers. Nanocomposites made of cost-effective polysaccharides with eco-friendly, inorganic clay minerals exhibit outstanding hybrid performance and have been recognized as one of the best available green materials of the 21st century.[1] These novel, environmentally- friendly materials represent new avenues for biodegradable polysaccharides with potential applications in medicine, coatings, automotive, packaging, environmental protection, and other relevant fields.[2-4]

Chitosan (CS) is the second most abundant natural amino polysaccharide. It is mainly extracted from marine biowaste, such as shrimp and crab shells.[5-7] Favored for properties such as biodegradability, biocompatibility, antimicrobial effects, good film formation, and high positive charge,[8,9] CS is widely used in food production, bacterial inhibition, tissue engineering, pharmaceuticals, cosmetics, and other applications.[10-17] Due to low water solubility, poor thermal stability, and weak antibacterial properties under neutral and alkaline conditions, however, CS use remains substantially limited. In effort to broaden the material's potential application, Wang and other researchers intercalated CS into rectorite (REC), a new type of layered silicate which exhibits high mechanical and thermal resistance, good colloidal properties in water, and strong absorptivity, obtaining intercalated chitosan/rectorite nanocomposites in 2 days via conventional heating; but the interlayer spacing was only increased by 1 nm compared to REC itself.[18] Generally, interlayer spacing is one of the most notable features of REC because it influences the extent to which CS intercalates, the morphology of the intercalation, or the degree of exfoliation of the system. Chitosan/organic rectorite nanocomposites have attracted considerable interest as far as good intercalation and excellent comprehensive properties, due to the fact that modified REC has larger interlayer spacing and lower surface energy favorable for forming intercalated nanocomposites. At present, the materials are typically prepared under traditional heating conditions, the reaction time for which is 6-48 h and the reproducibility of which is quite poor.

The microwave irradiation method, invented by Gerda in 1986, is quicker and more simple than other, similar methods.[19] Kabiri and other researchers prepared CS-based clay nanocomposites within several minutes using microwave irradiation.[20,21] In this study, an attempt was made to prepare chitosan/organic rectorite nanocomposites in a convenient, efficient, and homogeneous way via microwave irradiation method.

Prior to this study, relatively few reports appear on the interaction mechanism between CS and organic rectorite (OREC), or the effects of CS characteristics, such as molecular weight on the properties of chitosan/organic rectorite nanocomposites. To this effect, another important goal of the present study was to investigate the effects of CS molecular weight on the properties of chitosan/organic rectorite

MOE Key Laboratory of Wooden Material Science and Application, Beijing Forestry University, Qinghua East Road 35, Haidian 100083, Beijing, China. E-mail: yuzhiming@bjfu.edu.cn; bjfuzhangyang@bjfu.edu.cn

nanocomposites. Two chitosans with high and low molecular weight (CSH and CSL) were selected to prepare two types of chitosan/organic rectorite nanocomposites (CSHOR and CSLOR). The morphology and crystallization behavior, thermal stability, and antibacterial properties of CSHOR and CSLOR were determined to study the effects of CS molecular weight and identify the CS that most effectively allows intercalation into OREC layers.

Experimental section

Materials

Two chitosans with high and low molecular weights were sourced from Zhejiang Biochemical Co. (Taizhou, China). For simplicity, the molecular weights calculated from GPC were denoted as CSH (Mw 590 kDa) and CSL (Mw 3 kDa) and their degree of deacetylation was 92%. Calcium rectorite (REC) refined from clay minerals was provided by Hubei Mingliu Inc., Co. (Wuhan, China). The purity (95%) of the sample was verified by elemental analysis. Gemini surfactant was purchased from Henan Daochun Chemical Technology Co., Ltd. (Henan, China). An XH-100B microwave synthesis system was obtained from Beijing Xiang-Hu Technology Co., Ltd. (Beijing, China). Fig. 1 shows the chemical structure of CS[22] and Gemini surfactant. All other reagents were of analytical grade.

Synthesis of organic rectorite

Organic rectorite (OREC) was prepared under microwave irradiation by exploiting the ion-exchange reaction between REC and Gemini surfactant. Four grams of REC powder was dispersed in distilled water under ultrasonic stirring for 30 min, and the clay suspension was left for 60 h. 100 mL 1.5% (w/v) Gemini surfactant isopropanol solution was dropped slowly into the clay suspension and reacted under microwave irradiation for 800 W and 85° C for 60 min. The final product was obtained by centrifugation and washed with 50% (v/v) isopropanol aqueous solution until Cl^- could not be identified by 0.1mol/L $AgNO_3$ solution. Finally, the resultant OREC was freeze-dried at -60° C and ground in an agate mortar.

Preparation of chitosan/organic rectorite nanocomposites

Chitosan/organic rectorite nanocomposites were prepared as follows: the OREC powder obtained above was dispersed in 50% (v/v) isopropanol aqueous solution to obtain a 1% (w/v) clay suspension after ultrasonication for 30 min. CSH and CSL were dissolved in acetic acid to prepare a 1% (w/v) solution (pH=5), then were added slowly into the pretreated OREC suspension and reacted via microwave irradiation at 800 W and 80° C for 75 min. The synthetic nanocomposites were next freeze-dried at -60° C, then ground into powder. An overview of the prepared nanocomposites and their designations is provided in Table 1.

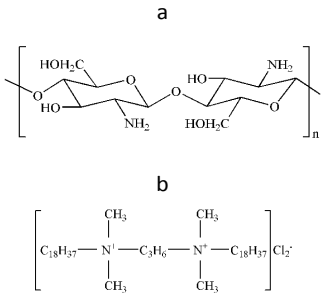

Fig. 1 Chemical structure of (a) CS and (b) Gemini surfactant.

Table 1 Chitosan/organic rectorite nanocomposites used in this study

Nanocomposite designation	Mass ratio (CS:OREC)	Molecular weight (Intercalated CS)
CSHOR	4:1	590 kDa
CSLOR	4:1	3 kDa

Characterization

Small angle X-ray diffraction (SAXRD) patterns of the powder samples were measured using a D8 advance X-ray diffractometer (Bruker, Germany) with an area detector operating under a voltage of 40 kV and a current of 40 mA using Cu-Kα as the source (λ= 0.15418 nm). The relative intensity was recorded in the scattering range (2θ) of 1-10° at a scanning speed of 1°/min.

Fourier transform infrared (FT-IR) spectra were gathered on a Vertex 70v FT-IR spectrophotometer (Bruker, Germany) at room temperature by the KBr pellets method. Each spectrum was acquired with a resolution of 4 cm^{-1} and a spectral range of 400 - 4000 cm^{-1}.

Zeta potential was determined by Zetasizer Nano ZS typed nanometer particle size and potential analyzer (Malven, England), with a sample concentration of 0.1% (w/v). In aqueous media, pH is one of the most important factors that affect zeta potential. In order to avoid the effect of the acetic acid, used as chitosan solvent, on the zeta potential of the nanocomposites, the pH of all test solutions was adjusted to 5 by acetic acid prior to testing. Three replicates were conducted for each group and the average values were reported.

Surface morphology was visualized and evaluated via an SU8010 field emission scanning electron microscope (FESEM, Hitachi, Japan) with an acceleration voltage of 15 kV. The powder samples were mounted on a sample holder fixed with double-sided adhesive tape. Before observation, the samples were sputter coated with a thin layer of gold. The microstructures were observed using a HT7700 transmittance electron microscope (TEM, Hitachi, Japan) at an accelerating voltage of 100 kV. Samples for TEM analysis were dispersed in 50% ethanol solution and dropped on Cu mesh grids, then dried in an oven at 50° C for 10 min.

Crystallization behavior test

The effects of CS molecular weight on crystallization behavior of obtained nanocomposites were determined by wide angle X-ray diffraction (WAXRD). The experiment was performed using a

diffractometer type D8 advance (Bruker, Germany) with Cu Kα (λ= 0.15418 nm) radiation at 40 kV and 40 mA. The scanning rate was 2°/min, ranging from 5-45°.

Thermal stability experiment

Thermal stability was evaluated by thermogravimetric analysis (TGA) using a TGAQ50 typed thermal analyzer (TA, USA). TGA and DTG thermograms were obtained in the temperature range of 30 to 700° C under nitrogen and with ramp rate of 10 °C/min.

Antibacterial assay

To study the antibacterial properties of CSHOR and CSLOR, gram-positive *Staphylococcus aureus* (provided by the Chinese Academy of Sciences) served as model pathogenic bacteria. Six antibacterial suspensions were diluted to appropriate concentrations in phosphate buffer (pH7.2), and 10 mL of each sample was added to sterile petri dishes with 10 mL nutrient agar. *Staphylococcus aureus* was adjusted by sterile distilled water to 10^7cfu/ml. The bacterial suspension of 2μl was then inoculated on the prepared nutrient medium-containing antibacterial suspension and incubated at 37° C. The minimum inhibition concentration (MIC) values were measured after a 24 h culture.

MIC is defined as the lowest concentration required to inhibit the growth of bacteria, i.e. the concentration at which no bacterial colony is visible.

Results and discussion

Structure characterization of organic rectorite

The ordered structure of materials can be successfully determined by SAXRD methods. SAXRD patterns of REC and OREC are shown in Fig. 2. The d001 peak of OREC shifts towards lower angle in comparison with REC, indicating the successful modification of Gemini surfactant. Based on Bragg's equation, nλ =2dsinθ, the interlayer distance was calculated at

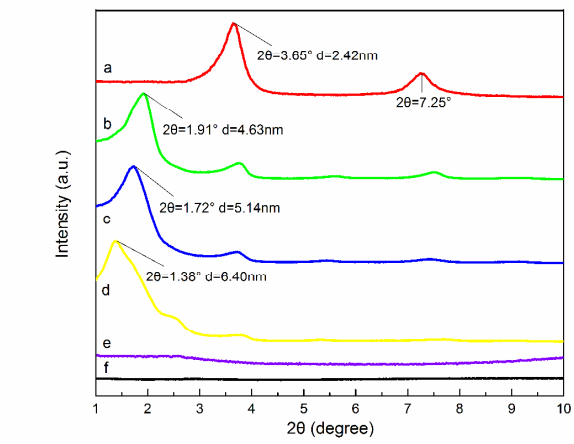

Fig. 2 SAXRD patterns of (a) REC, (b) OREC, (c) CSHOR, (d) CSLOR, (e) CSH and (f) CSL.

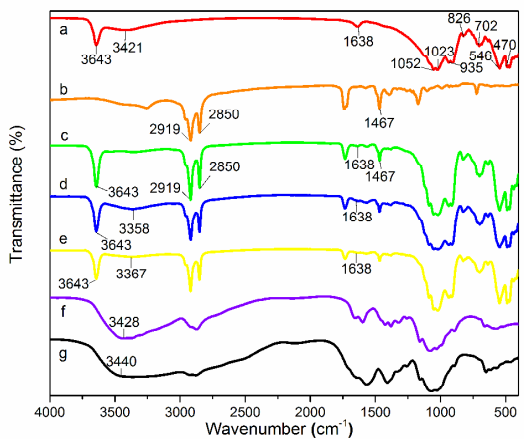

Fig. 3 FT-IR spectra of (a) REC, (b) Gemini surfactant, (c) OREC, (d) CSHOR, (e) CSLOR, (f) CSH and (g) CSL.

2.42 nm for REC and 4.63 nm for OREC, confirming that Gemini surfactant was successfully incorporated into the REC interlayer.

In order to verify the OREC structure, FT-IR spectra were investigated as shown in Fig. 3. The characteristic peaks of REC are as follows: Al–OH stretching vibration band at 3643, 935, and 702 cm^{-1}, H-O-H stretching vibration peak at 3421 cm^{-1}, H-O-H bending vibration peak at 1638 cm^{-1}, Si–O stretching vibration peak at 1052 and 1023 cm^{-1}, and Si–O bending vibration at 546 and 470 cm^{-1}. In the OREC spectrum shown in Fig. 3c, the characteristic peaks of REC appear. Two stronger adsorption bands appear at 2919 and 2850 cm^{-1}, which are belonging to the $-CH_2$ antisymmetric stretching vibration and symmetric stretching vibration peaks of Gemini surfactant, confirming the cationic exchange reaction between Ca^{2+} of REC and organic cations of Gemini surfactant.[23] In addition, another new peak at 1467 cm^{-1} is ascribed to C-H bending vibration peak of Gemini surfactant. The fact implies the formation of OREC.

Interaction between chitosan and organic rectorite

SAXRD patterns of OREC, CSH, CSL, CSHOR and CSLOR are shown in Fig. 2. The original CSH and CSL do not show any diffraction peaks in the range of 1-10°, while the OREC-reinforced nanocomposites show diffraction peaks at 2θ around 1.72° and 1.38°, respectively. As compared to OREC, the interlayer distances of CSHOR and CSLOR are around 5.14nm and 6.40nm, as calculated by the Bragg's equation, which are larger than that of OREC itself. The enlarged interlayer distance of CSHOR and CSLOR suggests that CSH and CSL had been inserted into the OREC interlayers successfully.

FTIR spectra of OREC, CSH, CSL, CSHOR and CSLOR are shown in Fig. 3. In the characteristic peaks of CSH and CSL, the broad absorption peak at 3428 cm^{-1} for CSH and 3440 cm^{-1} for CSL correspond to the coupling stretching vibrations of N–H and O–H groups. Differently, the broad absorption peak is wider and shifts to the lower frequency in the spectra of CSHOR and CSLOR, indicating that hydrogen bond interactions exist at the external surface of OREC with the adsorbed CSs (representing CSH and CSL).[24,25] This is consistent with a previous study which found

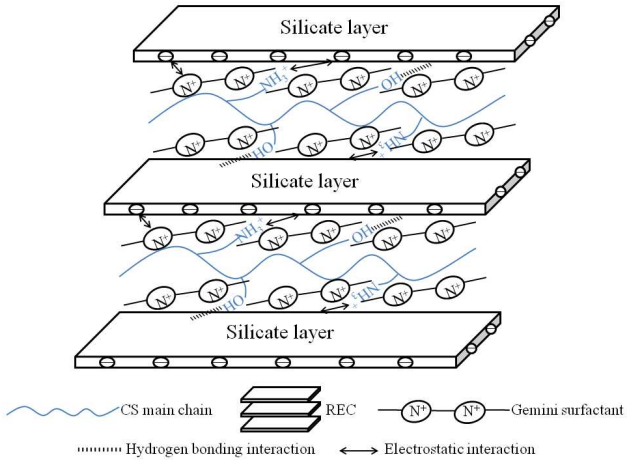

Fig. 4 Schematic of the intercalation mechanism of obtained nanocomposites.

that hydroxyl groups on an OREC surface were able to interact with a polymer substrate to form a new interface layer or partial network structure.[18,26] In the OREC spectrum, the characteristic peak at 3643 cm^{-1} belongs to the stretching vibration of hydroxyl groups, and the peak at 1638 cm^{-1} is ascribed to the bend vibration of the water band; these are weaker in the CSHOR and CSLOR spectra. This phenomenon likely occurred where negatively charged –OH on the surface of OREC had electrostatically interacted with $–NH_3^+$ in CSs.

Zeta potential is an important physical property exhibited by any particle in suspension that can be used to characterize the electrostatic surface of suspensions and emulsions. The zeta potentials of REC, OREC, CSH, CSL, CSHOR and CSLOR are listed in Table 2. REC is a negatively-charged surface with a zeta potential value of -27.8 ± 0.4 mV. The intercalation of Gemini surfactant into REC neutralizes part of the negative charge, yet OREC charge is remains negative. The zeta potential values for CSH and CSL are +56.1 ± 0.3 mV and +60.3 ± 0.6 mV, respectively. The intercalation of CSH and CSL into OREC finally creates a positively-charged surface on CSHOR and CSLOR. The potential value of CSHOR is not the simple addition of the value of OREC and CSH, while CSLOR's is not the simple addition of the value of OREC and CSL, revealing that CSs effectively covered the surface of OREC layers, as well as the strong electrostatic interaction between CSs and OREC, which is in accordance with the FT-IR results.

All the above results indicate that there were hydrogen bonding and electrostatic interactions between CS and OREC after which CS was intercalated into the OREC structure.[27] The intercalation mechanism of the obtained nanocomposites is illustrated in Fig. 4.

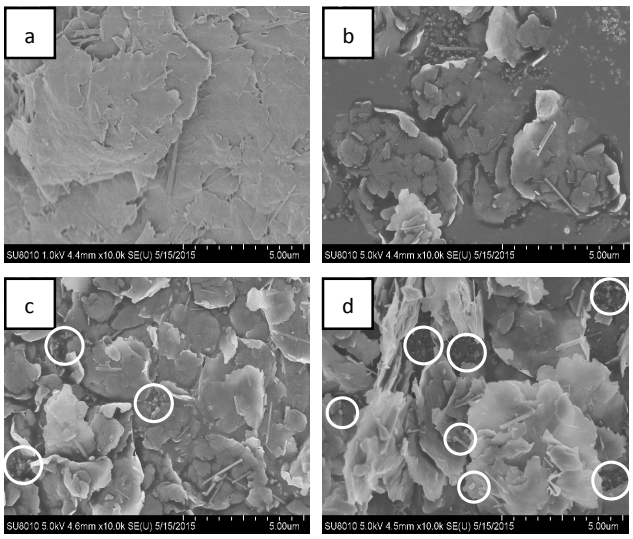

Fig. 5 FESEM micrographs of (a) REC, (b) OREC, (c) CSHOR, and (d) CSLOR.

Effect on morphology and crystallization behavior

Fig. 5 shows the surface morphology of REC, OREC, CSHOR and CSLOR under 10,000x magnification. The FESEM micrographs detail a remarkable change in the structure of the REC surface. The surface of pure REC has an irregular, flaky morphology (Fig. 5a), whereas that of OREC (Fig. 5b) is covered by uniform particles and possesses loosely arranged layers, indicating that OREC was successfully formed. Images of CSHOR and CSLOR are displayed in Fig. 5c and 5d, in which most of the REC maintains the layered structure and CSLOR exhibits favorable dispersion and looser structure in comparison with CSHOR. Furthermore, compared to CSHOR (Fig. 5c), more particles (particles marked with white circles represent CSs and partial Gemini surfactant) are attached to the surfaces and edges of REC layers in CSLOR (Fig. 5d). All the preceding observations suggest that CSL exhibits better interaction with OREC. It can be speculated that, as molecular weight decreases, the capacity of CS to interact with OREC increases.

Transmission electron micrographs provide quantitative information regarding morphology and internal structure of nanocomposites.[28] TEM images provided in Fig. 6 exhibit typical morphology of layered REC, OREC, CSHOR and CSLOR, in which the dark lines correspond to REC layers, while the bright areas represent CSs and partial Gemini surfactant. Compared to OREC and CSHOR, CSLOR showed broader interlayer distance in its TEM micrograph. Interlayer spacing was measured to be about 6.4 nm, which coincides with the SAXRD analysis. More CSL are inserted into the interlayer of OREC than CSH, where the bright areas are larger for CSLOR than CSHOR in the image; this observation can likely be attributed to the effect of molecular weight. The molecular weight of CSL is lower, meaning CSL has shorter chain length than CSH, thus CSL chains have more freedom due to weaker intramolecular hydrogen bonds. In that case, larger driving force for intercalation can be obtained; hence, CSL can easily intercalate into OREC interlayers to enlarge the interlayer spacing compared to CSH.

In order to investigate the effects of CS molecular weight on the crystalline properties of obtained nanocomposites, WAXRD patterns of samples from 5° to 45° were obtained as shown in Fig. 7. The diffraction pattern of OREC consists of five main

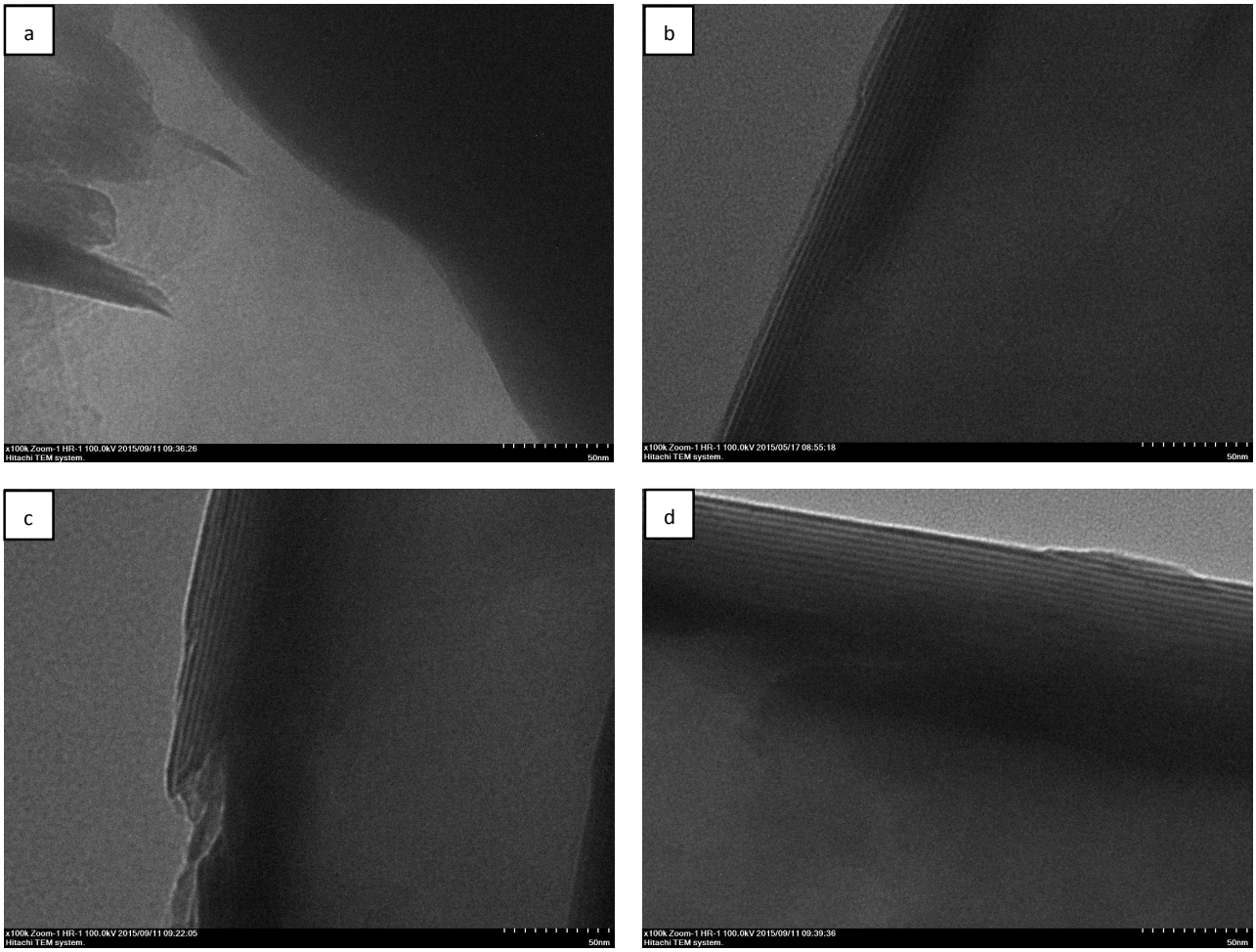

Fig. 6 TEM micrographs of (a) REC, (b) OREC, (c)CSHOR and (d) CSLOR.

crystalline peaks at 7.40°, 18.50°, 20.07°, 27.51°, and 35.26°, while neat CSH and CSL show two major characteristic crystalline peaks, which describe crystallinity behavior,[29,30] respectively at around 10.95°, 19.92° and 9.52° 21. 58°. The diffraction pattern of CSHOR is the combination of OREC and CSH, while CSLOR is the combination of OREC and CSL. OREC diffraction peaks in CSHOR and CSLOR remained visible, while their intensity weakened in comparison with pure OREC. The crystal structure of CSH and CSL is not obvious in CSHOR and CSLOR, confirming that CSs interacted strongly with layered OREC and intercalated into the interlayer successfully, resulting in significant changes in CSs crystallization. Compared to CSHOR, the corresponding diffraction heights in the WAXRD pattern of CSLOR are lower, especially the crystalline peaks at 7.40°, 18.50°, and 27.51° and the peak at 7.40° shifts towards high angle. Most likely, due to the intercalation of CSH and CSL into the OREC interlayers, the ordered multilayer morphology of OREC remained present but the interlayer distance increased in varying degrees, influencing the crystallization properties of CSHOR and CSLOR. From the above of analyses, it is apparent that the intercalated CSs and OREC formed strong interactions, and that the crystallization behavior of obtained nanocomposites is closely related to CS molecular weight.

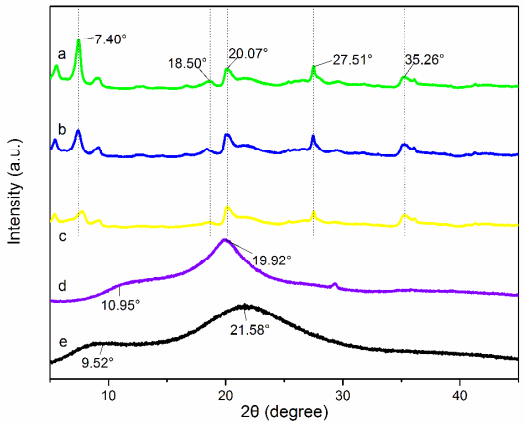

Fig. 7 WAXRD patterns of (a) OREC, (b) CSHOR, (c) CSLOR, (d) CSH and (e) CSL.

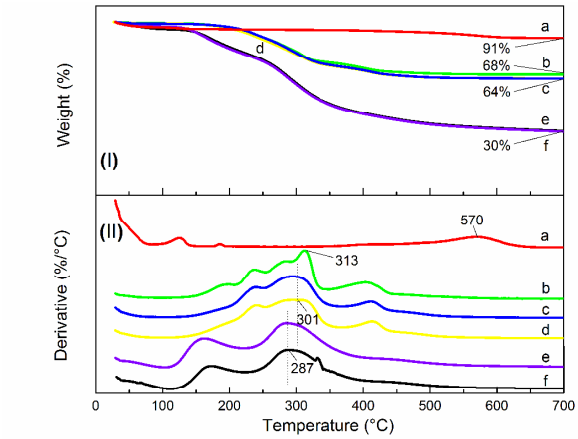

Fig.8 TG curves of (a) REC, (b) OREC, (c) CTSOR, (d) CTOOR, (e) CSH and (f) CSL, I: TGA curves; II: DTG curves.

Thermal stability analysis

TGA and DTG curves of REC, OREC, CSH, CSL, CSHOR and CSLOR are shown in Fig. 8. TGA results indicate that REC is thermally more stable than neat CSH and CSL; only 9% of REC is decomposed up to 700° C. By contrast, CSH and CSL show low thermal stability, with residual weight at 700° C of only 30% and T_{max} (the temperature at which the rate of weight loss reaches a maximum) at about 287° C. The T_{max} of CSHOR and CSLOR increased by 14° C compared to CSH and CSL, and 64% of both CSHOR and CSLOR remained at 700° C. These results demonstrate that CSHOR and CSLOR have higher thermal stability than CSH and CSL, and remain unaffected by CS molecular weight, evidenced by the fact that there is almost no distinction between TGA and DTG results of CSHOR and CSLOR.

In this case, improved thermal stability likely occurred due to many factors. For one, REC, which includes a mica layer, has high temperature resistance expected to enhance the thermal stability of nanocomposites.[31,32] As well, when CSs are in a restrained gallery space of the layered structure, the fractional free volume of CSs becomes smaller,[33] the hydrogen bonding and electrostatic interactions which cause poor mobility of CSs may be attributed to thermal stabilization of CSs. In addition, REC layers with high aspect ratio act as barriers that considerably reduce the volatility of decomposed pyrolysis products and limit the continuous decomposition of CSs.[34]

As shown in Fig. 8, the T_{max} and remnant weight of CSLOR did not increase significantly compared to CSHOR; this may have occurred due to insufficient interlayer distance growth, at which REC could not provide remarkable better protection for CSL and thus failed to greatly reinforce the thermal performance of CSLOR.

Antibacterial activity

Inhibitory effects of REC, OREC, CSH, CSL, CSHOR and CSLOR against *Staphylococcus aureus* were measured based on MIC. As shown in Table 2, pure REC has no antimicrobial activity, while neat CSH, CSL and OREC show slight inhibitory effect;

Table 2 Zeta potential and MICs of REC, OREC, CSH, CSL, CSHOR, and CSLOR

Sample code	Zeta potential (mV, n=3)	MICs (%, w/v, n=3)
Blank	-	-[a]
PBS	-	-
REC	-27.8±0.4	-
OREC	-3.7±1.2	1
CSH	+56.1±0.3	3
CSL	+60.3±0.6	2.5
CSHOR	+2.0±0.2	0.04
CSLOR	+10.5±0.8	<0.01

[a]No antibacterial properties.

conversely, both CSHOR and CSLOR exhibit significant inhibition of bacteria. Fig. 9 exhibits the morphology of *Staphylococcus aureus* colonies after treatment with OREC, CSH, CSL, CSHOR and CSLOR at a concentration of 0.01%, as compared to the control. As shown in Fig. 9, CSLOR completely inhibited *Staphylococcus aureus* growth. In contrast, CSHOR only inhibited *Staphylococcus aureus* to a limited extent. Additionally, the MIC value of CSLOR is lower than CSHOR's, indicating that the antimicrobial activity of CSLOR is stronger than CSHOR.

Zeta potential results shown in Table 2 indicate that CSH and CSL are positively-charged polyelectrolytes, and thus could interact vigorously with negatively-charged bacteria at the cell surface, change bacterial cell membrane permeability, restrain the growth of cells, and even kill cells.[35,36] Previous studies have reported that REC possesses certain adsorption capacities, i.e., it can adsorb and fix bacteria.[37] Gemini surfactant can produce hydrophobic effect on bacteria to further reinforce the adsorption capacity of REC. The antibacterial activity of CSHOR and CSLOR may be divided into two stages: first, adsorb and immobilize bacteria on the surface of REC, while the second stage is related to the accumulation of CSs in the interlayer of REC; CSs chains were orderly and aggregated when confined in the interlayer of REC, positive charge (amino groups) density per

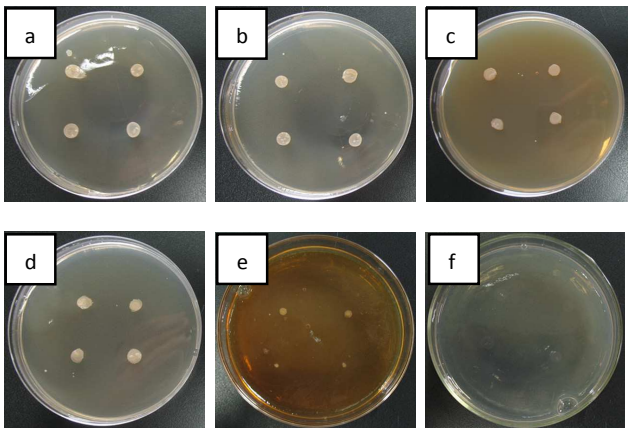

Fig. 9 Appearance of colonies of Staphylococcus aureus after treatment with OREC, CSH, CSL, CSHOR and CSLOR at a concentration of 0.01%: (a) blank, (b) OREC, (c) CSH, (d) CSL, (e) CSHOR and (f) CSLOR.

unit volume may increase, accordingly, the stronger interaction between amino groups and bacteria may occur.[38] Because nanocomposites can combine both advantages of layered silicates and polymers, their antimicrobial properties in this study improved compared to OREC, CSH and CSL.

The antimicrobial activity of nanocomposites was observed to improve alongside decreasing CS molecular weight. CS with low molecular weight showed enhanced positive zeta potential value of nanocomposites, which benefits its interaction with negative bacteria surface; CS with low molecular weight also more readily intercalated into OREC layers. These phenomena were confirmed by TEM images and SAXRD patterns, where the increase of interlayer spacing induced greater bacterial absorption while allowing more CS to react with the bacteria.

Conclusion

Two nanocomposites, CSHOR and CSLOR, were successfully prepared and characterized in this study using OREC and chitosans with high and low molecular weight. The interlayer spacing was increased to 5.14 nm and 6.40 nm, respectively, in CSHOR and CSLOR. Compared to the conventional heating method, nanocomposites were successfully obtained by microwave irradiation heating method much faster. Results showed that CS and OREC connected through hydrogen bonding and electrostatic interaction, and that the thermal stability and antibacterial properties of both CSHOR and CSLOR significantly improved compared to CSH and CSL.

This study altogether suggests that OREC can be used as an enhancer for improving the performance of CS to expand its potential applications. Furthermore, the results of this study suggest that CS molecular weight is an important factor in its intercalation into OREC. The interlayer distance of OREC increased with decreasing CS molecular weight, which resulted in changes in morphology and crystallization behavior and enhanced antibacterial activity without impacting thermal stability. CS with low molecular weight exhibited better intercalation into OREC layers.

Acknowledgements

The authors would like to express their gratitude to the National Science & Technology Pillar Program during the Twelfth Five-year Plan Period (2012BAD24B02) for providing research funds.

References

1 S. S. Ray and M. Bousmina, *Prog. Mater. Sci.*, 2005, **50**, 962-1079.
2 N. Bitinis, M. Hernández, R. Verdejo, J. M. Kenny and M. Lopez-Manchado, *Adv. Mater.*, 2011, **23**, 5229-5236.
3 E. Ruiz-Hitzky, P. Aranda, M. Darder and M. Ogawa, *Chem. Soc. Rev.*, 2011, **40**, 801-828.
4 X. Wang, X. Pei, Y. Du and Y. Li, *Nanotechnology*, 2008, **19**, 375102.
5 N. A. Burns, M. C. Burroughs, H. Gracz, C. Q. Pritchard, A. H. Brozena, J. Willoughby and S. A. Khan, *RSC Adv.*, 2015, **5**, 7131-7137.
6 R. Weska, J. Moura, L. Batista, J. Rizzi and L. Pinto, *J. Food. Eng.*, 2007, **80**, 749-753.
7 I. Younes, M. Rinaudo, *Mar. Drugs.*, 2015, **13**, 1133-1174.
8 R. Hejazi, M. Amiji, *J. Control. Release.*, 2003, **89**, 151-165.
9 C. Pillai, W. Paul and C. P. Sharma, *Prog. Polym. Sci.*, 2009, **34**, 641-678.
10 P. Dutta, S. Tripathi, G. Mehrotra and J. Dutta, *Food. Chem.*, 2009, **114**, 1173-1182.
11 H. Tang, P. Zhang, T. L. Kieft, S. J. Ryan, S. M. Baker, W. P. Wiesmann and S. Rogelj, *Acta. Biomater.*, 2010, **6**, 2562-2571.
12 I.-Y. Kim, S.-J. Seo, H.-S. Moon, M.-K. Yoo, I.-Y. Park, B.-C. Kim and C.-S. Cho, *Biotechnol. Adv.*, 2008, **26**, 1-21.
13 P. H. Chua, K. G. Neoh, E. T. Kang and W. Wang, *Biomaterials*, 2008, **29**, 1412-1421.
14 M. R. Kumar, R. A. Muzzarelli, C. Muzzarelli, H. Sashiwa and A. Domb, *Chem. Rev.*, 2004, **104**, 6017-6084.
15 S. K. Samal, M. Dash, F. Chiellini, X. Wang, E. Chiellini, H. A. Declercq and D. L. Kaplan, *RSC Adv.*, 2014, **4**, 53547-53556.
16 A. Cooper, N. Bhattarai, F. M. Kievit, M. Rossol and M. Zhang, *Phys. Chem. Chem. Phys.*, 2011, **13**, 9969-9972.
17 Z.-M. Huang, Y.-Z. Zhang, M. Kotaki and S. Ramakrishna, *Compos. Sci. Technol.*, 2003, **63**, 2223-2253.
18 T. Feng, L. Xu, *RSC Adv.*, 2013, **3**, 21685-21690.
19 R. Gedye, F. Smith, K. Westaway, H. Ali, L. Baldisera, L. Laberge and J. Rousell, *Tetrahedron. Lett.*, 1986, **27**, 279-282.
20 K. Kabiri, H. Mirzadeh and M. J. Zohuriaan-Mehr, *Iranian. Polym. J.*, 2007, **16**, 147.
21 H. El-Sherif and M. El-Masry, *Polym. Bull.*, 2011, **66**, 721-734.
22 J. Wang, Y. Chen, Y. Wang, S. Yuan, G. Sheng and H. Yu, *RSC Adv.*, 2012, **2**, 494-500.
23 Y. Huang, X. Ma, G. Liang and H. Yan, *Chem. Eng. J.*, 2008, **141**, 1-8.
24 K. Kabiri, H. Mirzadeh and M. Zohuriaan-Mehr, *J. Appl. Polym. Sci.*, 2010, **116**, 2548-2556.
25 H. Deng, X. Li, B. Ding, Y. Du, G. Li, J. Yang and X. Hu, *Carbohydr. P olym.*, 2011, **83**, 973-978.
26 X. Wang, Y. Du, J. Yang, X. Wang, X. Shi and Y. Hu, *Polymer*, 2006, **47**, 6738-6744.
27 R. Xu, X. Feng, W. Li, S. Xin, X. Wang, H. Deng and L. Xu, *J. Biomat. Sci.- Polym. E.*, 2013, **24**, 1-14.
28 S. Pavlidou and C. Papaspyrides, *Prog. Polym. Sci.*, 2008, **33**, 1119-1198.
29 W. Li, X. Li, Y. Chen, X. Li, H. Deng, T. Wang, R. Huang and G. Fan, *Carbohydr. Polym.*, 2013, **92**, 2232-2238.
30 P.-H. Chua, K.-G. Neoh, E.-T. Kang and W. Wang, *Biomaterials*, 2008, **29**, 4314-4322.
31 K.-C. Cheng, C.-B. Yu, W. Guo, S.-F. Wang, T.-H. Chuang and Y.-H. Lin, *Carbohydr. Polym.*, 2012, **87**, 1119-1123.
32 Y. Lu, X. Li, X. Zhou, Q. Wang, X. Shi, Y. Du, H. Deng and L. Jiang, *RSC Adv.*, 2014, **4**, 33355-33361.
33 Z. Wang, B. Wang, N. Qi, H. Zhang and L. Zhang, *Polymer*, 2005, **46**, 719-724.
34 L. Yu, L. Li, Z. Wei and F. Yue, *Radiat. Phys. Chem.*, 2004, **69**, 467-471.

35 2 M. Kong, X. G. Chen, K. Xing and H. J. Park, *Int. J. Food. Microbiol.*, 010, **144**, 51-63.
36 H. Liu, Y. Du, X. Wang and L. Sun, *Int. J. Food. Microbiol.*, 2004, **95**, 147-155.
37 X. Wang, Y. Du, J. Luo, J. Yang, W. Wang and J. F. Kennedy, *Carbohydr. Polym.*, 2009, **77**, 449-456.
38 X. Wang, Y. Du, J. Luo, B. Lin and J. F. Kennedy, *Carbohydr. Polym.*, 2007, **69**, 41-49.

